Development of 3D printed nanomaterials for restoration of exterior artworks

Development of 3D printed nanomaterials for restoration of exterior artworks

E. Mansi[1], G. Terranova[1], D. Linardi[2], S. Marfia[2], E. Monaldo[2], M. Ricci[2], M. Imbimbo[3], A. Pelliccio[4], A. Brunetin[5], R. D'Amato[1*]

1. ENEA, Fusion and Technologies for Nuclear Safety and Security Department, FSN-TECFIS-MNF, C.R. Frascati, Via Enrico Fermi, 45 - 00044 Frascati (RM), Italy
2. Roma TRE University, Dept. of Civil Engineering, Computer Science and Aeronautical Technologies, Via Vito Volterra 62 - 00146 Roma, Italy
3. University of Cassino and Southern Latium, Dept. Civil and Mechanical Engineering, Viale dell'Università – loc. Folcara –snc, 03043, Cassino (FR), Italy
4. University of Cassino and Southern Latium, Dept. Literature and Philosophy, Viale dell'Università – loc. Folcara –snc, 03043, Cassino (FR), Italy
5. Nadir Plasma & Polymers Srl, Via Don F. Tosatto 15, 30174 Mestre (VE) Italy

*rosaria.damato@enea.it

Abstract. Despite the great potential of 3D printing technologies coupled with nanotechnologies, just few studies are present in the scientific literature. Application of nanocomposites materials for 3D printing in the field of cultural heritage restoration, is a promising approach to obtain novel and functionalized materials for the artworks element to be recreated. In this context, the present work aims to study innovative nanocomposites materials suitable for the considered application. A commercial PLA filament was additivated with SiC, SiO_2 and TiO_2 nanoparticles, synthetized by CO_2 laser pyrolysis. Nanocomposite filaments were produced by a co-rotating twin-screw extruder and specimens were produced by 3D printing and analysed against their mechanical and hydrophobic properties by means of tensile tests and water absorption and contact angle measurements, respectively.

1. Introduction

In recent years, polymer based Additive Manufacturing (AM) processes undergo to a significant increase thanks to the development of 3D printing technologies and new extrusion processes for polymeric materials, in particular the Fused Deposition Modeling (FDM) [1][2]. In fused deposition processes, the thermoplastic polymer filament is heated, extruded and finally deposited layer by layer on a printing surface following a predetermined path established in the design phase. A wide range of research topics and new applications and methods are continuously developed [2]; for example Seeram *et al.* investigated the possibility to use AM for medical devices and tissue engineering [3], while Wu *et al.* studied AM materials employed in the construction industry [4]. Main advantages of the AM are related to the 3D printing technique versatility and to the possibility to reproduce complex geometries directly from a computer-aided design model; both low cost and high-performance functionalized materials can be obtained [2].

As a raw material in FDM, PLA (polylactic acid) is the most broadly used thermoplastic filament because of it is biodegradable, recyclable, biocompatible, and bioresorbable. Applications of additively manufactured PLA element are widespread in medical, food, and textile industries. However, PLA has

several drawbacks from a mechanical point of view, including low fracture toughness and low impact strength, and also in terms of durability. These weaknesses limit the use of PLA in some applications.

FDM can be used not only for printing prototype plastic parts in a cost-effective way, but it can be exploited in order to produce stronger fiber (micro and nano-sized) reinforced composite materials [5,6]. Among them, the integration of nanotechnology with AM has the potential both to enhance existing techniques and to create nanocomposites, which possess unique properties [7] strongly depend on the size of nanostructures [8]. These nanostructured material characteristics allow applications in different areas, such as chemical and biological sensing [9], catalysis [10], electrochemicals [11] and therapeutics and diagnostics [12]. Banks *et al.* reported an overview of the main achievements within the field of additive manufactured conductive polymers and nanocomposites for high electrical conductivities applications [13], while Vogt *et al.* studied the increasing in mechanical properties of a biorenewable polymer functionalized with nanofibers as filler [14].

Between the new sceneries and possibilities in the AM field, cultural heritage is a very promising application thanks to the increase of accuracy reached by current technologies. In the last years AM has been effectively applied for the reproduction of artworks, for museum exhibitions and for supporting CH restoration. This evolution of instruments and methods is in partnership with a diffusion of instrumental techniques for surveys, such as the 3D scan, which allows observation of complex geometries impossible to analyse through traditional methods. Replicas can be used in many ways: for study and research, for setting up alternative museum exhibitions, such as tactile museum tours for the blind and visually impaired, for restoration, re-creating missing portions of an object, for organization of workshops with schools and for museum merchandising (*e.g.* producing with cheap reproduction technologies accurate small-scale replicas of the artworks conserved in a museum or in a CH institution) [15]. Ullah *et al.* developed an analytical method for creating a point-cloud for modelling, applied to preserve artifacts having cultural significance [16].

In the last years, nanotechnologies are successfully employed in preservation and restoration of cultural heritage [17]. Artifacts are often exposed to humidity and to harsh environmental chemical and biological conditions; there are a lot of study for Titanium dioxide (TiO_2) and Silicon dioxide (SiO_2) nanoparticles to be used for the restoration and consolidation of archaeological artifacts thanks to their photocatalytic and hydrophobic properties. Photocatalytic and self-cleaning properties of TiO_2 nanopowders allow to use nano-TiO_2-based coating on historic architectural stone surfaces, in order to obtain a self-cleaning treatment able to reduce pollution and deterioration effects preserving their original visual appearance [18–21]. SiO_2 nanoparticles show hydrophobic properties that can be used to give super hydrophobicity to stone surfaces of monuments [22–24]. Silicon carbide (SiC) nanomaterials show remarkable mechanical properties; SiC nanocrystals were used to study nanocomposites coatings with high resistance to aggressive environments [25], and were also tested as fillers dispersed into an aluminosilicate brick matrix [26].

Functionalized products can be obtained coupling the 3D printing with nanotechnologies. Although the very promising results that could be achieved by coupling nanotechnologies and AM, there is a lack of literature data in cultural heritage applications, to the best of our knowledge.

In this work 3D printing technologies, enhanced with nanotechnologies, are for the first time, evaluated for applications in cultural heritage restoration. At this purpose commercial PLA filament was additivated with 3% of three different ceramic nanopowders (SiC, SiO_2 and TiO_2) and three obtained nanocomposites filaments have been used to realize 3D printed specimens. The influence of nanoparticles on mechanical features has been investigated by means of tensile tests highlighting the changes with respect to the 3D printed parts with raw PLA. Also, hydrophobic properties of printed specimens are evaluated and compared with the commercial, non additivated, PLA behaviour.

2. Experimentals

All the solvents and chemicals are reagent grade and were supplied by Sigma-Aldrich, while all the gases are pure >99,99% and were supplied by SIAD srl.

Nanoparticles were synthetized by CO_2 laser pyrolysis technique. TiO_2 and SiO_2 nanoparticles were

prepared starting by liquid precursors, titanium isopropoxide $Ti[OCH(CH_3)_2]_4$ (TTIP) and tetraethyl orthosilicate $Si(OC_2H_5)_4$ (TEOS) respectively, with ethylene C_2H_4 gas as sensitizer and Ar as confinement gas. SiC nanoparticles were prepared starting by silane SiH_4 and acetylene C_2H_2 gases with Ar as confinement gas.

Experimental set-up (Figure 1) is equipped with a CW CO_2 laser beam (wavelength 10.6 μm) focused by spherical lens, the maximum laser power is 1.2 kW with a density in the reaction volume up to 275 kw/cm^2. An Ar flow confines and cools down the particles. The set-up is also equipped with a pressure control unit and a mass flow meters system. Thanks to an evaporation system, nanopowders can be produced starting both by liquid and gaseous reagents, the heater can work up to 200 °C. Further details are described in D'Amato et al. [27]. Reaction parameters are reported below. This technique requires that at least one of the precursors are sensitive to laser radiation, otherwise a sensitizer is added to the reagents flow, as in the case of ethylene in SiO_2 and TiO_2 synthesis. Synthetised nanopowders are collected in a filter bag and a thermal treatment post synthesis could be required in order to eliminate carbon impurities.

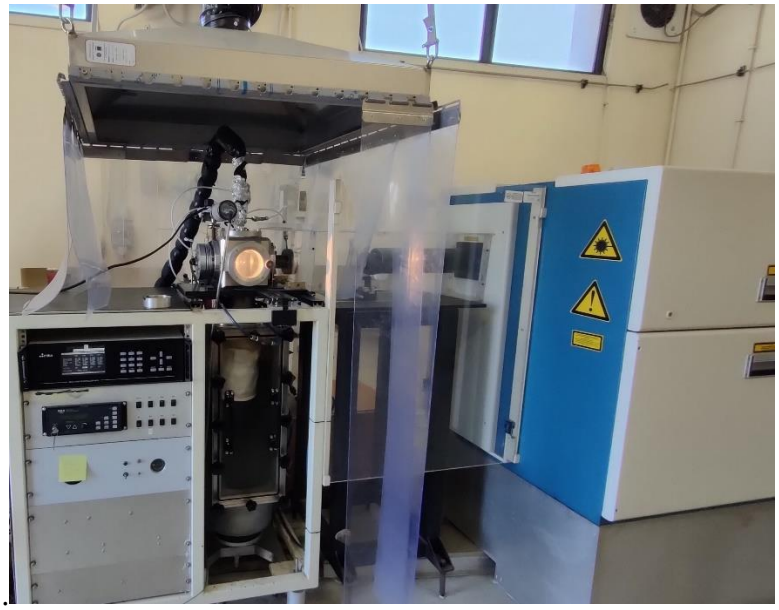

Figure 1. CO_2 laser pyrolysis facility for nanopowders synthesis

The thermoplastic polymer is PLA (poly-lactic acid) standard with neutral color provided by FILOALFA [28], as a filament having diameter of 1.75 mm.

Nanocomposites were manufactured starting by PLA filament: three filaments made of nanocomposites with 3% w/w of SiC or SiO_2 or TiO_2 nanoparticles were realised, that is PLA+SiC, PLA+SiO_2 and PLA+TiO_2, respectively. The PLA filament was cut to small pellets that were dried at 80 °C in vacuum for 3 hours before use. Manufacturing was carried out by using a Thermo Scientific co-rotating twin-screw extruder (Process 11) equipped with 11 mm screws diameter (ratio length/diameter:40) (Figure 2) by a two-step process; the first one leads to nano loaded PLA pellets (2×1.5 mm), while in the second step the nanocomposite filament is produced. The profile screw (Figure 2) used in both production steps is characterized by three mixing zones designed to reach a high level of dispersion and distribution of nanopowder in the polymer matrix minimizing the thermal-mechanical degradation of PLA during the process. All nanocomposite filaments were dried at 55°C for 4 hours in vacuum and stored in sealed pack.

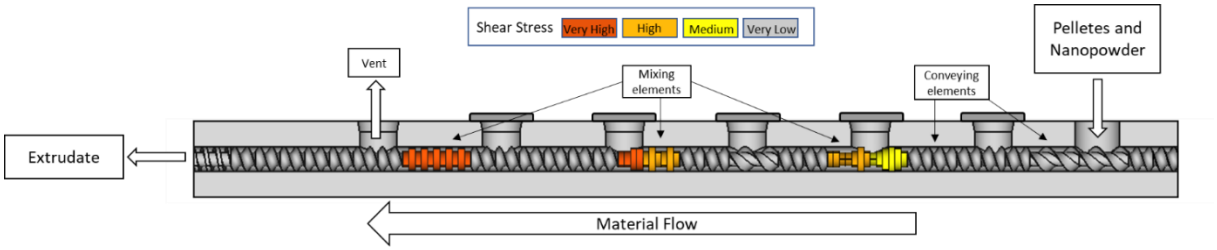

Figure 2. Extruder screw profile used to produce nanocomposite pellets and calibrated filaments

The specimens for mechanical characterization were designed using the Autodesk Fusion 360 software and then the file was elaborated via the RAISE3d slicer software ideaMaker [29]. The samples were printed with the 3D printer RAISE3D Pro2 Plus equipped with a nozzle of 0.4 mm in diameter and setting an infill value of 100% and a flow rate percentage of 120%. The nozzle speed was set equal to 50 mm/s. The hot-end temperature was equal to 215 °C and the bed temperature was 60 °C. 24 samples with rectangular shape and dimensions equal to 250×30×1.2 mm (length x width x thickness) were realized. The rectangular shape was preferred with respect to the dog-bone shape, in order to avoid a premature failure due to stress concentrations at the offset contours of filaments near the fillet radius, that usually occur in the dog-bone samples. The same build orientation was considered for all the samples, with the filament orientation aligned to main dimension of the sample in all the layers. The tests were carried out to evaluate the elastic mechanical parameters, thus the perimeters were not added to the samples because their direction would be different from the main filament orientation. Moreover, the layers were added one after the other along the smallest dimension of the sample. Thus each sample had 6 layer of thickness equal to 0.2 mm.

IR analyses were performed with a Perkin-Elmer Spectrum100 FTIR spectrophotometer equipped with and ATR module in order to study the chemical and morphological nanoparticles and nanocomposites structures. BET measurements were carried by using Monosorb (Quantachrome instrument), a single point surface area analyzer, leading to evaluate the particles diameter [30].

The tensile tests were realized with an MTS machine instrumented with a 100 kN load cell. A displacement control was applied with a quasi-static loading speed equal to 0.5 mm/min [31] and the test was stopped when the sample achieved the failure. The procedure is similar to that carried out in [32, 33].

Water absorption measurements were carried out according to international standard ISO 62:2008 [34]. Test specimens previously dried in desiccator, were immersed in distilled water, and taken out from the water, dried with paper towel and weighed, according to scheduled timetable. Every measure was repeated 6 times.

Static contact angle measurements of printed specimen were performed with an experimental set-up developed by ENEA according with literature data [35, 36]. Set-up was composed by an optic module equipped with an Dinolite optical microscope, a sample holder and a light box. Contact angle measurements were performed by a droplet of water placed on the samples horizontal surface; a syringe was used to drop 50 µl of water for each measurement. Results were analyzed with the contact angle plug-in developed for the IMAGEj image editing software [37, 38]. This plug-in calculates the contact angle of a drop on a flat surface using the sphere and the ellipse approximation.

3. Results

3.1 Nanoparticles Synthesis

Nanoparticles were synthetized by CO_2 laser pyrolysis technique, a gaseous phase synthesis process which permits to obtain pure nanoparticles with a high productivity and narrow size distribution thanks to the highly localized and fast heating in a small, confined reaction volume [25].

The SiC nanoparticles were prepared starting by a mixture of SiH_4, which is a strong absorber of CO_2 laser radiation, and C_2H_2. In order to produce pure SiC nanopowders, the reactive gases were

injected into the chamber in molar proportion 2:1 using mass flow controllers. The mean nanoparticle size can be varied in the range 20–50 nm by acting on the process parameters, in particular the laser power density, the reagent flows, the total pressure in the reaction chamber and the inner nozzle diameter. For this work, the following process parameters were used: the pressure in the reaction chamber was set at 8.0×10^4 Pa, the silane flow was set at 500 sccm, acetylene flow at 250 sccm and the Ar flow, which ensures the confinement of the reaction, at 5 slm, laser power was set at 630 W.

Pure SiO_2 nanoparticles were obtained starting by a liquid precursor, *i.e.* TEOS, with a vapor pressure of about 130 Pa, in which Si atoms are already oxidized. Since TEOS is not a strong absorber of laser radiation, ethylene gas (C_2H_4) was added as a reaction sensitizer; its resonant absorption at about 10 μm with a relatively high dissociation energy led to increase the coupling of the laser energy in the system. Ar was bubbled into the TEOS tank to leak TEOS as aerosol to the reaction chamber and Ar was also used as reagents diluent. The evaporator was settled at T_{ev} = 170 °C. C_2H_4 and TEOS aerosol were mixed just before the exit of the inlet nozzle (6 mm in diameter). The laser power density was set at 900 W, the TEOS flow = 50 g/h, C_2H_4 flow = 100 sccm, the total pressure in the reaction chamber = 5.3×10^4 Pa. The synthesized SiO_2 powders had carbon contamination coming from TEOS and/or unwanted ethylene decomposition. To remove these contaminants, it was necessary to perform a thermal treatment in air at T = 600 °C for 6 h.

TiO_2 nanopowder was produced by vapors of TTIP, in the presence of ethylene as sensitizer. Typical reaction parameters were: evaporator temperature T_{ev} = 180 °C, TTIP flow = 45 g/h and ethylene flow = 400 sccm, laser power = 1200 W and pressure in the chamber = 4.7×10^4 Pa. As SiO_2 nanoparticles, prepared TiO_2 were contaminated by free carbon, mostly coming from TTIP and unwanted ethylene dissociation, carbon contamination was removed by thermal treatment in air (5 hours at 500°C).

Table 1 reports the synthesis productivity, together with BET results. Productivity of around 60 g/h and reaction yields near to 100% was found for SiC. Regarding nano SiO_2 and TiO_2 productivity of 12 g/h and 11 g/h was obtained, respectively.

Synthesized nanoparticles were characterized by BET technique; the size of SiC nanoparticles was determined to be of about 25 nm, while 10 nm and 13 nm particles diameters were obtained for SiO_2 and TiO_2 nanoparticles, respectively.

Table 1. Productivity and BET results for nanoparticles.

Sample	Productivity (g/h)	Specific surface (m^2/g)	d (nm)
TiO_2	11	107.3	13
SiO_2	12	221.7	10
SiC	58	75.7	25

Chemical characterization was performed by FTIR spectroscopy; Figure 3 reports IR spectra acquired on nanopowders samples. Spectra show that synthetized nanoparticles were pure and free of contaminant. IR analysis of TiO_2 nanoparticles let us define their morphological structure: the peak at around 450 cm^{-1} is related to the O-Ti-O bonding in anatase structure [39] (Figure 3a). For SiO_2 nanoparticles, IR spectrum (Figure 3b) shows a strong absorption at 1100 cm^{-1} with a weaker band at 809 cm^{-1} which correspond to Si-O stretching of the opaline type. SiC IR spectrum shows the typical band at 830 cm^{-1} (Figure 3c) due to Si-C stretching.

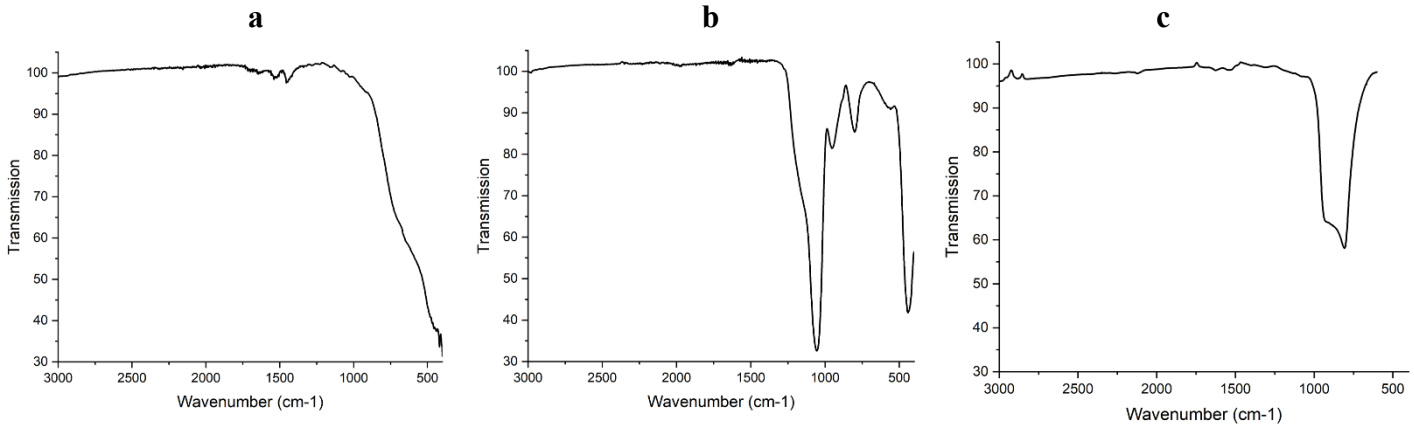

Figure 3. Infrared spectra of produced nanoparticles. From left: TiO_2 (a), SiO_2 (b) and SiC (c)

3.2 Nanocomposites Preparation

Synthesized nanoparticles were used to produce nanocomposite materials: commercial PLA filament was loaded with a 3% w/w of SiO_2, TiO_2 and SiC nanoparticles by extrusion method and three different filaments were produced PLA+SiO_2, PLA+TiO_2 and PLA+SiC, respectively. Our aim was to test how the presence of different ceramic nanopowders influence technological performances of 3D printed nanocomposites and if nanoparticles can induce functional features to commercial PLA. We choose SiO_2 for hydrophobic properties, TiO_2 for photocatalytic and self-cleaning behaviour and SiC for mechanical characteristics.

Three nanocomposite filaments to use as feedstock in 3D printer (FFF) were produced by a two-step process (Figure 4). In the first step nanopowder and PLA pellets were feed in the extruder and, after cooling in water bath, the extrudate was pelletized and the collected nanocomposite pellets were used to produce the calibrated filament in the second process step.

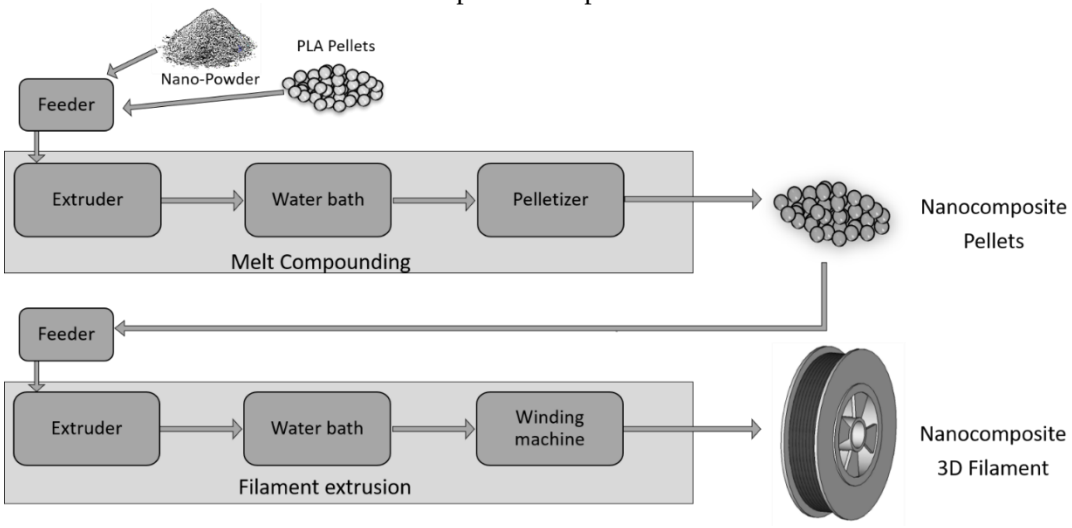

Figure 4 Process flow diagram of nanocomposites production

The advantage of two-step process over a single step process, where raw materials are directly transformed in calibrated filament, is that different process parameters (Table *2*) could be set for mixing process (First step) and filament production (Second step).

Table 2 Extrusion process parameters set to produce nanocomposite compounds (First step) and calibrated filament (Second step)

	Speed (rpm)	**Zone temperature (°C)**								**Mass Rate (g/min)**
First step	150	190	190	190	200	200	200	200	200	9
Second step	150	190	190	190	200	200	190	185	170	5

No relevant problems occurred during the extrusion production and, in particular, the melt strength of the nanocomposite extrudates were high enough to permit to easily manage the filament during cooling step.

Raw PLA and nanocomposites filaments were then used for producing specimens by 3D-printing to test their properties, as described below. Printed specimens were also characterized by FTIR and the spectra (Figure 5) resulted to be very similar each other. It can be evinced that the PLA chemical structure was not affected by nanopowders presence.

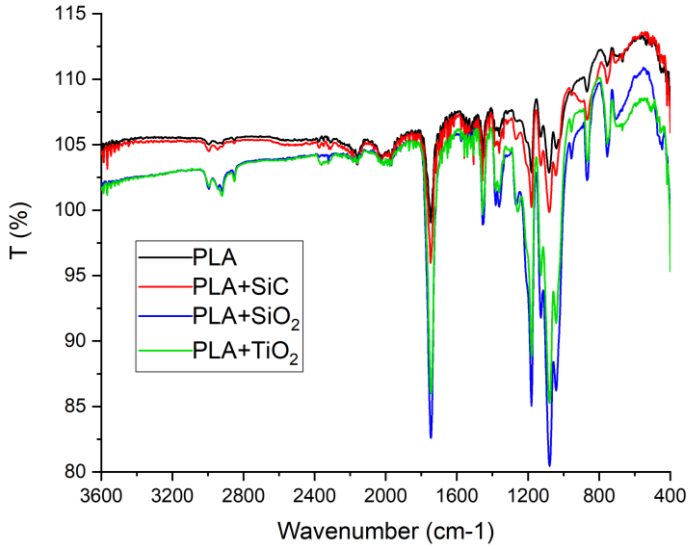

Figure 5. Infrared spectra of specimens made by: PLA (black), PLA + SiC (red), PLA + SiO_2 (blue) and PLA+TiO_2 (green)

3.3 Mechanical characterization

The experimental program comprised 20 tensile tests. Figure 6 reports the averages of the stress-strain curves obtained for each type of sample: PLA standard, PLA+SiC, PLA+TiO_2 and PLA+SiO_2. Moreover, the stress-strain curves for the PLA samples additivated with nanoparticles are reported. The stress measure σ is derived as the ratio between the force values recorded during the tensile test and the initial cross-sectional area of the specimen. The strain measure ε is obtained from the ratio between the applied displacement and the free length of sample, *i.e.* the length of sample between the gripped regions in the testing machine [40]. The results show that in all cases, the mechanical response was characterized by an initial linear phase followed by a short nonlinear branch interrupted by the occurrence of the brittle failure of the samples. Considering only one type of sample, the results of the five tensile tests are homogeneous. Only in the case of PLA+TiO_2 samples, the stress-strain curves show different behaviour in the nonlinear region. Looking the average curves, results reveal that SiC and SiO_2 nanoparticles did not significantly affect the elastic stiffness of the sample, with an increase by 3.3% and a decrease by

1.2%, respectively. Thus, the presence of nanoparticles had a positive effect on the mechanical properties of the samples. In both cases, the ultimate strain increased by 5.5-10%. Conversely, the TiO_2 nanoparticles determined a decrease in elastic stiffness equal to the 10% and a decrease in the ultimate strain equal to the 8%. The causes of this behaviour should be further investigated.

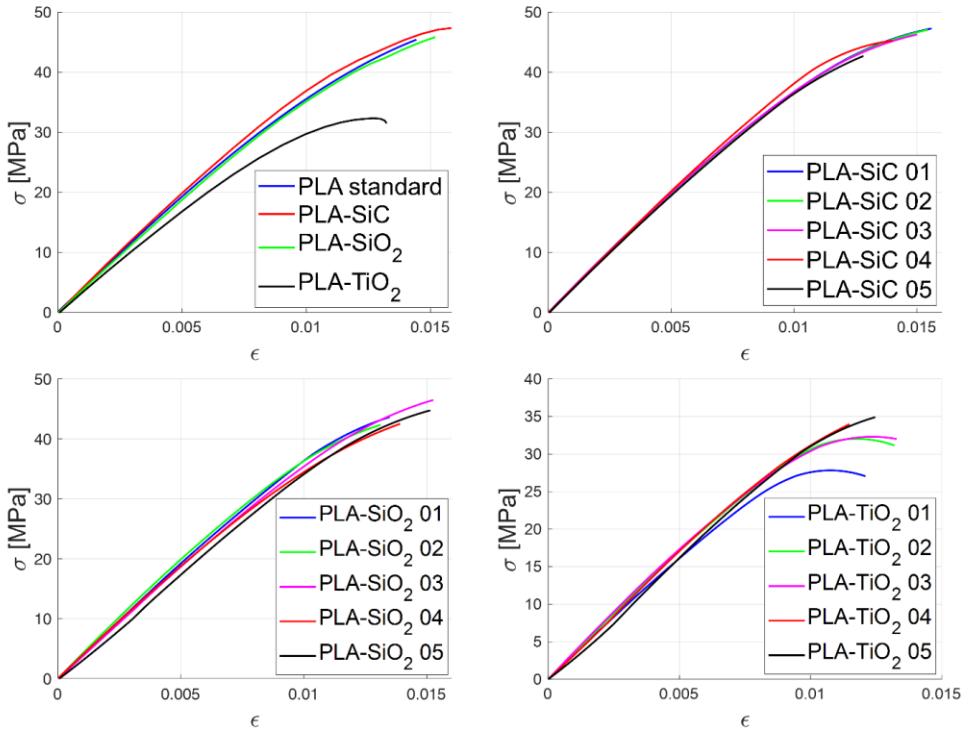

Figure 6 Comparison between the average tensile stress–strain curves and stress-strain curves for composites samples.

3.4 Water absorption measurements

International standard ISO 62:2008 [34] describes procedures for determining the amount of water absorbed by plastic specimens of defined dimensions, when immersed in water. Test specimens, consisting of three replicas of printed polymer and nanocomposites, were immersed in distilled water at room temperature, for prescribed periods. The amount of water absorbed by each test specimen was determined by measuring its change in mass, *i.e.* the difference between its initial mass and that after exposure to water, the change being expressed as a percentage of the initial mass.

For each test specimen, the percentage change in mass (CIP) relative to the initial mass is calculated by using the following equation (Equation 1):

$$CIP_i = \frac{m_i - m_o}{m_o} * 100 \qquad \text{Equation 1}$$

where m_o is the initial mass of the test specimen, in grams (g), after initial drying and before immersion and m_i is the mass of the test specimen, in grams (g), after immersion for *i* hours. Results are expressed as the arithmetic mean of the three values obtained at the same exposure duration. Experimental error is estimated according to error analysis.

Moreover, protection ratio (PR), which indicates the effect of nanoparticles on materials absorption properties, was evaluated as follow (Equation 2):

$$PR = \frac{CIP_0 - CIP_t}{CIP_0} * 100 \qquad \text{Equation 2}$$

where CIP_t and CIP_0 are, respectively, nanocomposites and PLA water absorption coefficient

corresponding to the longest test duration.

Water absorption tests were carried out on printed specimens of commercial PLA and three nanocomposites. For each exposure time the CIP coefficient was calculated and the results are reported in Figure 7. From these data we have obtained absorption curves; the plot slopes are related to the absorption kinetic, while the plateau value can be considered the water saturation value. It can be noted that all samples show an initial sharp increase of the absorption coefficient and that these values reach a plateau within the first 24 hours. An exception is given by PLA+TiO_2 sample, which CIP continued to increase during test. A comparison between nanocomposites and PLA shows how nanoparticles affect the material behaviour; it can be evinced as PLA+SiO_2 exhibit more hydrophobic behaviour compared to printed PLA, while PLA+TiO_2 showed an increased hydrophilicity. Also, the SiC presence induce an increasing in the material hydrophilicity. The calculated PR shows a hydrophobicity increasing of around 50% for printed PLA additivated with SiO_2 while for the TiO_2 and SiC nanocomposites a negative protection ratio indicates a decreasing in the material hydrophobic properties.

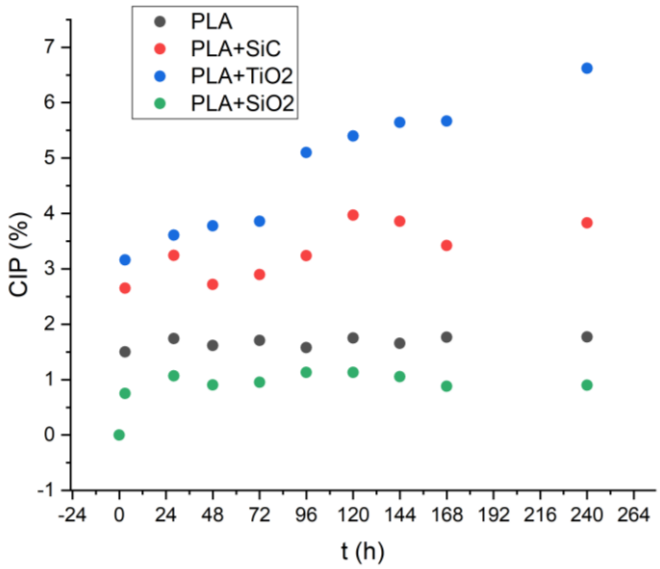

Figure 7. Water absorption results of tested samples: PLA (black), PLA + SiC (red), PLA + SiO_2 (green) and PLA+TiO_2 (blue)

FTIR spectra were performed on printed specimens before and after water absorption tests in order to verify if PLA or nanocomposites underwent to degradation due to hydrolysis. In literature it is reported that an intensity decrease of the C=O band at 1750 cm^{-1} indicate PLA hydrolysis [41]. Obtained spectra do not show any decreasing or shift of the C=O band, that indicates that nanocomposites did not undergo to a significant degradation.

3.5 Contact angle measurements

The wettability properties of the nanocomposite coatings were assessed by static water contact angle measurements to evaluate the local water repellence of the surface specimens.

As an example, the image of water drop on PLA specimen, is reported in Figure 8a, while Figure 8b reports the related analysis performed with the ImageJ plug-in employed for contact angle calculation. Measured contact angle values for all the specimens are reported in Table 3. All the specimens showed a contact angle < 90°, typical of a hydrophilic behaviour. However it can be evinced as the presence of nanopowders slightly induced an increase of contact angle, improving the surface hydrophobicity of tested materials.

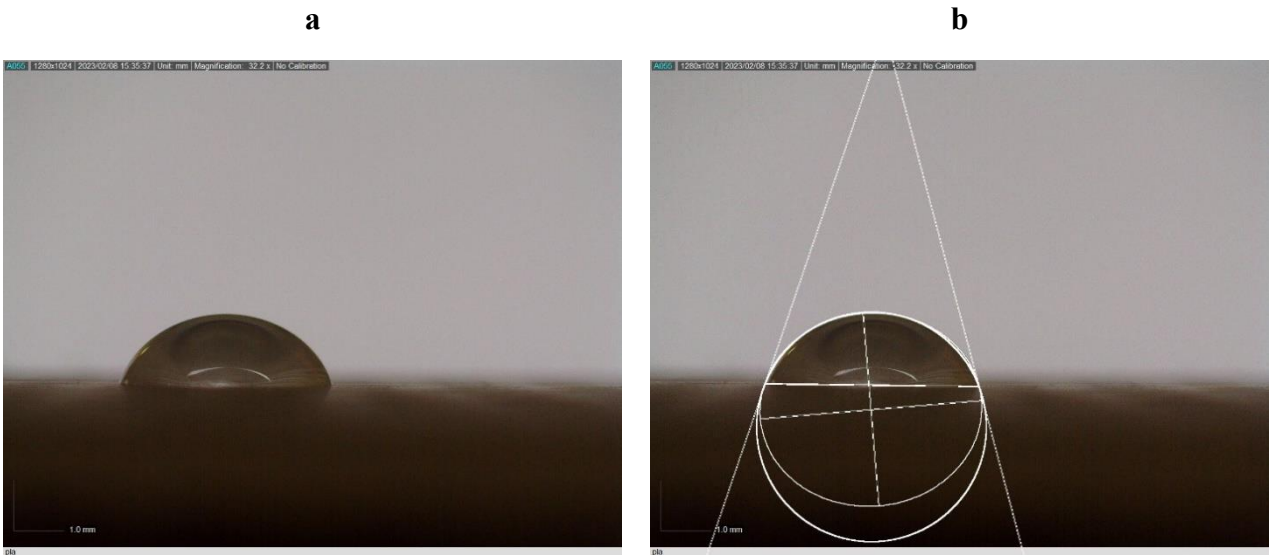

Figure 8. Contact angle measurements: image acquired with a contact angle meter set-up on a PLA sample (a) and analyzed image (b)

Table 3. Measured contact angles

Samples	**CA (degrees)**
PLA	73.2
PLA+TiO_2	74.9
PLA+SiO_2	76.8
PLA+SiC	76.1

4 Conclusions

In this paper three polymeric nanocomposites based on PLA and containing oxides nanoparticles, that is SiO_2, TiO_2 and SiC were obtained as filament for 3D print and their mechanical performance and hydrophobicity behaviour were characterized in view of their application for integrative restoration in Cultural Heritage.

The mechanical behaviour of 3D printed PLA-based samples has been investigated by means of tensile tests. The influence of three different types of nanoparticles has been analysed. Results reveal that SiC and SiO_2 nanoparticles do not affect significantly the mechanical properties of the samples. In particular, the presence of SiC nanoparticles determines an improvement both in terms of elastic stiffness and ultimate strain. However, the presence of TiO_2 nanoparticles has a negative influence on the performance of the 3D samples.

Hydrophobic behaviour was investigated by means of water absorption and contact angle measurements. The best results were obtained for SiO_2 nanocomposite, that shows positive protection ratio respect to PLA standard. It is worth noting that all the nanoparticles led to an increase of contact angle, probably due to a roughness surfaces induced by nanoparticles presence.

These are the first results of the investigation. Further studies should be carried out considering also the influence of the printing parameters and what happens if the percentage of nanoparticles present in printed material is increased.

Acknowledgments
This study is funded by Regione Lazio, Progetti di Gruppi di Ricerca 2020 - POR FESR Lazio 2014–2020, Italy, project: 3DH-solutions - Soluzioni di Stampa 3D per il recupero strutturale e architettonico di beni culturali (CUP F85F21001530009).
Elisabetta Monaldo acknowledges the funding by Italian Ministry of University and Research (MUR) within the Programma Operativo Nazionale Ricerca e Innovazione PON 2014–2020 DM 1062/2021 fondo FSE-REACT-EU, azioni IV.4.
The authors wish also to thank Dr. Valentina Nigro and Antonella Lai, for her contribution in contact angle and IR measurements.

References
1. Monfared, V., Bakhsheshi-Rad, H. R., Ramakrishna, S., Razzaghi, M. & Berto, F. A brief review on additive manufacturing of polymeric composites and nanocomposites. *Micromachines* **12**, (2021).
2. Ngo, T. D., Kashani, A., Imbalzano, G., Nguyen, K. T. Q. & Hui, D. Additive manufacturing (3D printing): A review of materials, methods, applications and challenges. *Compos. Part B Eng.* **143**, 172–196 (2018).
3. Singh, S., Ramakrishna, S. Biomedical applications of additive manufacturing: Present and future. *Curr. Opin. Biomed. Eng.* **2**, 105–115 (2017).
4. Wu, P., Wang, J., Wang, X. A critical review of the use of 3-D printing in the construction industry. *Autom. Constr.* **68**, 21–31 (2016).
5. Jo, W., Yoon, B. J., Lee, H., Moon, M. W. 3D Printed Hierarchical Gyroid Structure with Embedded Photocatalyst TiO_2 Nanoparticles. *3D Print. Addit. Manuf.* **4**, 222–230 (2017).
6. Papon, E.A., Haque, A. Tensile properties, void contents, dispersion and fracture behaviour of 3D printed carbon nanofiber reinforced composites. *J. Reinf. Plast. Compos.* **37**, 381–395 (2018).
7. Olga S. I., Christopher B. W., T.A.C. Additive Manufacturing (AM) and Nanotechnology: Promises and Challenges. *Rapid Prototyping J.* **19** (5), 353-364 (2011).
8. Burda, C., Chen, X., Narayanan, R., El-Sayed, M.A., Chemistry and Properties of Nanocrystals of Different Shapes. *Chem. Rev.* **105**, 1025–1102 (2005).
9. Liu, S., Tang, Z., Nanoparticle assemblies for biological and chemical sensing. *J. Mater. Chem.* **20**, 24–35 (2010).
10. Monfared, V. *et al.* Catalysis with transition metal nanoparticles in colloidal solution: Heterogeneous or homogeneous? *Chem. Soc. Rev.* **38**, 21–31 (2009).
11. Sgobba, V., Guldi, D.M. Carbon nanotubes—electronic/electrochemical properties and application for nanoelectronics and photonics. *Chem. Soc. Rev.* **38**, 165–184 (2009).
12. Boisselier, E., Astruc, D. Gold nanoparticles in nanomedicine: preparations, imaging, diagnostics, therapies and toxicity. *Chem. Soc. Rev.* **38**, 1759–1782 (2009).
13. Ryan, K.R., Down, M.P., Hurst, N.J., Keefe, E.M., Banks, C.E. Additive manufacturing (3D printing) of electrically conductive polymers and polymer nanocomposites and their applications. *eScience* **2**, 365–381 (2022).
14. Herrero, M., Peng, F., Núñez Carrero, K.C., Merino, J.C., Vogt, B.D. Renewable Nanocomposites for Additive Manufacturing Using Fused Filament Fabrication. *ACS Sustain. Chem. Eng.* **6**, 12393–12402 (2018).
15. Balletti, C., Ballarin, M., Guerra, F. 3D printing: State of the art and future perspectives. *J. Cult. Herit.* **26**, 172–182 (2017).
16. Ullah, A.M.M.S., Watanabe, M., Kubo, A. Analytical point-cloud based geometric modeling for additive manufacturing and its application to cultural heritage preservation. *Appl. Sci.* **8**, (2018).
17. Giancristofaro, C., D'Amato, R., Caneve, L., Pilloni, L., Rinaldi, A., Persia, F. Performance of nanocomposites for preservation of artistic stones. *AIP Conf. Proc.* **1603**, 86–92 (2014).

18. Quagliarini, E., Bondioli, F., Goffredo, G. B., Licciulli, A., Munafò, P. Smart surfaces for architectural heritage: Preliminary results about the application of TiO_2-based coatings on travertine. *J. Cult. Herit.* **13**, 204–209 (2012).
19. La Russa, M. F. *et al.* Nano-TiO_2 coatings for cultural heritage protection: The role of the binder on hydrophobic and self-cleaning efficacy. *Prog. Org. Coatings* **91**, 1–8 (2016).
20. Kardar, P., Amini, R. Self-cleaning treatment on historical stone surface via titanium dioxide nanocoatings. *Pigment Resin Technol.* **48**, 404–408 (2019).
21. Goffredo, G. B., Quagliarini, E., Bondioli, F., Munafò, P. TiO_2 nanocoatings for Architectural Heritage: Self-Cleaning Treatments on Historical Stone Surfaces. *Proc. Inst. Mech. Eng. Part N J. Nanoeng. Nanosyst.* **228**, 2–10 (2014).
22. Manoudis, P. N. *et al.* Superhydrophobic films for the protection of outdoor cultural heritage assets. *Appl. Phys. A Mater. Sci. Process.* **97**, 351–360 (2009).
23. Barberio, M. *et al.* TiO_2 and SiO_2 nanoparticles film for cultural heritage: Conservation and consolidation of ceramic artifacts. *Surf. Coatings Technol.* **271**, 174–180 (2015).
24. Liu, Y., Liu, J. Design of multifunctional SiO_2–TiO_2 composite coating materials for outdoor sandstone conservation. *Ceram. Int.* **42**, 13470–13475 (2016).
25. D'Amato, R., Falconieri, M., Fabbri, V., Borsella, E. Perspectives of application for nanoparticles prepared by CO_2 laser pyrolysis: from ceramic nanocomposites to nanofluids. *Nuovo Cimento C* **36**, 11–22 (2013).
26. Conciauro, F., Filippo, E., Carlucci, C., Vergaro, V., Baldassarre, F., D'Amato, R., Terranova, G., Lorusso, C., Congedo, P.M., Scremin, B.F., Ciccarella, G. Properties of nanocrystals-formulated aluminosilicate bricks. *Nanomater. Nanotechnol.* **5**, 1–11 (2015).
27. D'Amato, R., Falconieri, M., Gagliardi, S., Popovici, E., Serra, E., Terranova, G., Borsella, E., Synthesis of ceramic nanoparticles by laser pyrolysis: from research to applications. J. Anal. Appl. Pyrolysis, **104**, 461-469 (2013).
28. FILOALFA. https://www.filoalfa3d.com/it/.
29. RAISE3D. https://www.raise3d.com/
30. Brunauer, S., Emmett, P. H., Teller, E. Gases in Multimolecular Layers. J. Am. Chem. Soc., **60 (**2), 309–319 (1938).
31. American Society for Testing and Materials. ASTM D638-14, Standard Practice for Preparation of Metallographic Specimens. *ASTM Int.* **82**, 1–15 (2016).
32. Alaimo, G., Marconi, S., Costato, L., Auricchio, F. Influence of meso-structure and chemical composition on FDM 3D-printed parts. *Compos. Part B Eng.* **113**, 371–380 (2017).
33. Monaldo, E., Ricci, M., Marfia, S. Mechanical properties of 3D printed polylactic acid elements: Experimental and numerical insights. *Mech. Mater.* **177**, 104551 (2023).
34. Standard, I. Plastics-Determination of water absorption, *Ref. number ISO* **62**, 2008 (2008).
35. Han, W., Shin, J., Ho Shin, J. Low-cost, open-source contact angle analyzer using a mobile phone, commercial tripods and 3D printed parts. *HardwareX* **12**, e00327 (2022).
36. Chen, H., Muros-Cobos, J. L., Amirfazli, A. Contact angle measurement with a smartphone. *Rev. Sci. Instrum.* **89**, (2018).
37. Stalder, A. F. *et al.* Low-bond axisymmetric drop shape analysis for surface tension and contact angle measurements of sessile drops. *Colloids Surfaces A Physicochem. Eng. Asp.* **364**, 72–81 (2010).
38. Williams, D. L. *et al.* Computerised measurement of contact angles. *Galvanotechnik* **101**, 2502–2512 (2010).
39. Bagheri, S., Shameli, K., Abd Hamid, S.B. Synthesis and characterization of anatase TiO_2 nanoparticles using egg white solution via Sol-Gel method. *J. Chem.* **2013**, 848205 (2013).
40. Monaldo, E., Marfia, S. Multiscale technique for the analysis of 3D-printed materials. *Int. J. Solids Struct.* **232**, 111173 (2021).
41. Lee, S. H., Song, W. S. Enzymatic hydrolysis of polylactic acid fiber. *Appl. Biochem. Biotechnol.* **164**, 89–102 (2011).